8th International Symposium

ROCKBURSTS AND SEISMICITY IN MINES

ALEXEY AND DMITRIY MALOVICHKO - EDITORS

RUSSIA. Saint-Petersburg - Moscow. 1-7 September 2013

8th Int. Symp. on Rockbursts and Seismicity in Mines, A. Malovichko & D. Malovichko (eds)

KEYNOTE LECTURE: NUMERICAL MODELING OF SEISMICITY: THEORY AND APPLICATIONS

A.M. Linkov
Rzeszow University of Technology, Rzeszow, Poland;
Institute for Problems of Mechanical Engineering, Saint Petersburg, Russia

Numerical modelling of seismic events is the basis for quantitative studying and interpretation of seismicity in well-established terms of solid mechanics. In this way we obtain a better basis for making decisions concerning with mining, rock burst mitigation, oil and gas exploration and production. The paper summarizes computational, geomechanical and geophysical rationale for progress in this area. We explain in detail how to employ the theoretical rationale for developing a computer code providing both mechanical quantities (stresses, strains, displacement, etc.) and seismic data (spatial and temporal distributions of events and seismic characteristics used in mining seismology). It is shown that a conventional code of the BEM, FEM, DEM or FPC type may be easily adjusted to simulations of seismic and aseismic events by complimenting it with a number of subroutines, described in due course. Examples illustrate applications to problems of mining and hydraulic fracturing.

In memory of the founder of synthetic mining seismicity, Professor Miklos Salamon

INTRODUCTION

A Little of History

Twenty years have passed since 1993, when Professor Miklos Salamon formulated the first theoretical rationale and practical application of synthetic mining seismicity. In fact, his key-note address to the 3rd International Symposium RaSiM (Salamon[1993]) contained all the germs of generality. He suggested as an urgent task for rock mechanics "*to evolve a tool which provides the opportunity of relating seismicity to the changing mining layout and to geological environment*". And what is especially significant, he suggested "*the method … to furnish the basis of such a tool*" (p. 299).

Further development has actually followed the line by Salamon. The only principal improvements consisted in including:

- Softening of a fractured element which, as shown by Cook[1965a, 1965b] (see also Hudson *et al*.[1972] and Linkov[1994]), provides a measure of brittleness and instability of rock.
- Time effects, which opens an opportunity to account for aseismic events and to model intervals between seismic events.

A natural way to account for time is to explicitly include creep into the constitutive equations. Napier and Malan[1997], Malan and Spottiswoode[1997] included the time explicitly into constitutive equations for *contact interaction* when numerically modeling seismicity. The contact was assumed to be viscoplastic. The authors employed the simplest viscous element in the programs DIGS, MINSIM, and MINF, what allowed accounting for aseismic effects. In addition to the mentioned dependences, the results included catalogues of synthetic seismicity and chains of events after a blast.

The advantages of this step included providing (under certain assumptions) the main seismic characteristics (location, energy, etc.) and agreement with observations. Nevertheless, in the cited papers, there were limitations as concerned with accounting for softening. The latter was used in a model, which includes a softening element *in parallel* with a viscous element. In accordance with the general theory (Linkov[2002]), the latter model exhibits fracture acceleration, but actually it ceases to generate instability in the form of a jump. It is because infinite instant stiffness of a viscous dash-pot prevents instability.

The simplest model capable to simulate both seismic and aseismic events is the Elasticity-Softening-Creep (ESC) model (Linkov[1997]). In this model, in contrast with that used previously, the softening element is included in series (not parallel) with the viscous (creeping) element. Its analysis shows (see, e.g. Linkov[1997, 2002]) that the ESC-model captures the most important effects: decaying aseismic deformation; smooth although accelerating aseismic deformation; and instant instability (seismic event). It appears that near a point of instant instability, there occur fracture acceleration and that arbitrary short time intervals may be observed near the point of dynamic instability. At the level of the earth crust, such aseismic accelerating movement appears as a so-called *silent earthquake* (see, e.g. Linder *et al*.[1996], Dragert *et al*.[2001] and Kawasaki[2004]). Revealing the existence of accelerating events fills the gap between slow creep and instant instability (seismic event).

Although models used differ in significant details, their employment has clearly demonstrated that synthetic seismicity mimics observed seismicity in the most essential features (Sellers and Napier[2001], Spottiswoode[2001], Linkov[2005, 2006]). As noted by Napier[2001]: "*… it appears that*

the explicit failure mode shows some superficial correspondence to observed seismic behavior but displays number of shortcomings".

Note that sometimes modeling in the line of Salamon is called "*active*", because it models *expected* events without employing the data on observed passed events. In contrast, "*passive*" modeling is based on employing data on events observed in a mine (e.g. Wiles *et al.*[2001]).

Passive modelling uses data on the location, orientation, radius of cracks and displacement discontinuities (DD), obtained from seismic monitoring. They serve as input data for numerical modeling of stress distribution on mining steps. The calculated stresses are used for conclusions on stability and for calibration of the model. The main problem of the passive approach is to transform seismic data into input information on the orientation of elements and values of the DD.

The applications of the passive approach look quite promising. As written in the paper by Wiles *et al.*[2001]: "*The authors believe that this technique provides a unique opportunity for construction of mine-wide stability models incorporating major structural factors*". The authors continue: "*Some would argue that since part of the rockmass behavior occurs aseismically, we cannot achieve this goal. We would argue that it is also true that part of rockmass behavior occurs seismically…*" Still the approach has obvious shortcomings: impossibility to use it on the stage of planning, neglecting aseismic events and difficulties with inversion of seismic data into the DD on cracks.

So far the active and passive approaches have been used separately. Meanwhile, nothing prevents to join them. In fact, this means calibration of the input data, used in direct modeling, by comparing the simulated events with the data of observation. Such joined geomechanical and seismic monitoring, discussed below, presents a challenge for modern science and practice.

Rock Mechanics and Seismicity: Advantages of Integration

Why is it important to join rock mechanics and seismicity? Let us recall merits and flaws of the two. Rock mechanics operates with concepts and quantities rigorously established in solid mechanics, such as displacement, strain, stress, equilibrium, stability, and the like. Consequently, if provided with reliable input data on rock structure, properties, contact and boundary conditions, it is possible to solve a problem by using modern computers and numerical techniques.

Unfortunately, the needed input information is limited and uncertain. For years, it has raised a doubt in practical usefulness of numerical simulations. As wrote Starfield and Cundall[1988]: "*…models (mathematical or computational) were generally thought to be either irrelevant or inadequate. Modellers spent a large part of their efforts trying to persuade skeptics that modeling was a useful engineering exercise*".

Uncertainty of input data distinguishes rock mechanics from other engineering fields. If following Starfield and Cundall[1988], we consider Holling's classification of sciences (Figure 1), we can see that our usual region is the region 2 of good understanding and little information.

In contrast, mining seismology provides vast data on seismic events while there are great difficulties in their interpretation in well-established terms of solid mechanics needed to make practical decisions. In Holling's classification, mining seismology is in the area 3 of vast data and poor understanding.

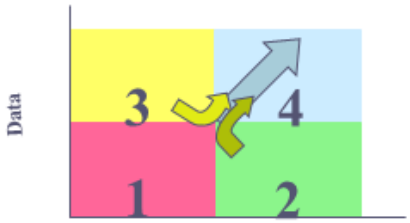

Figure 1. Holling's classification of sciences

Presently modern numerical techniques allow us to account for combined effect of thousands and even millions of structural elements and provide understanding of simulated processes. Meanwhile, there are no reliable input data on real rockmass. On the other hand, modern mining seismology processes millions of events, containing data on a rock state, while there is no proper understanding of the state. We see that the advantage of one tool is the shortcoming of the other. Clearly, their integration serves to cross-fertilization, which preserves their benefits and removes the flaws.

The scientific advantage of the integration consists in joining *rich data* of seismic monitoring with *clear understanding* of results of numerical simulation providing well-established mechanical quantities. This moves us into the area 4 on Figure 1 of sufficient data and better understanding.

Practical advantages are also obvious. We obtain a new modern tool for assessment of the state and processes in rocks and for making decisions. The tool allows us to carry out completely controlled seismological experiments, play various scenarios, calibrate input parameters, validate existing and suggest new methods serving for interpretation of seismic data. And what is also important, it is not expensive: actually, it is the work for a few specialists.

Recent Tendency: Joined Mechanical and Seismic Modelling and Monitoring in Real Time

An especial challenge is to use joined mechanical and seismic modeling and monitoring in real time. Nowadays,

the possibility to implement it is facilitated by tremendous progress in computers, numerical techniques, information technologies and automatic measurements. Actually, the passive approach contains the germs of the joined monitoring. It is visibly recognized by the specialists applying it, who wrote (Wiles *et al*.[2001]): "*The integration of deterministic modeling with seismic monitoring offers crucial data regarding local variability and sensitive features… Taken together this clearly enhances our deterministic prediction accuracy of rockmass response to mining*".

The feasibility of the purpose is evident from the papers by Cai *et al*.[2007] and Dobroskok *et al*.[2010]. The authors of the first of them used the FLAC and PFC for simulation of seismicity induced by large-scale underground excavations. The second work employed the code SEISM-3D, based on using the general theory (Linkov[2005, 2006]) in frames of the hypersingular boundary element method (H-BEM). The both papers vividly demonstrate that geomechanical and seismic modeling may be efficiently joined with daily seismic monitoring in mines. It provides important data for making reliable practical decisions.

The trend to meet the challenge is obvious from merging of ITASCA (geomechanics consulting and software development company) with ASC (Applied Seismology Consultants) in 2009. As advertised the site http://www.seismology.org/itasca_msapps.aspx (September 26, 2012), "*ASC and Itasca have developed advanced, groundbreaking techniques for correlating microseismic field observations with simulated microseismicity from Itasca's models*".

The same trend is also seen in transforming the ISS International by Dr. Mendecki into Institute of Mine Seismology (IMS) in 2011. The Institute, among other purposes, aims to compliment daily geomechanical calculations with numerical modeling of seismicity in real time and to compare the synthetic seismicity with the data of seismic monitoring.

The modeling of stressed state and seismicity joined with direct observations becomes of crucial significance for *hydraulic fracturing*. Hydraulic fracturing is widely used for stimulation of oil, gas and heat reservoirs. Its importance grows with the tendency to extract gas from low-permeable shales. The geomechanical data in these problems are even less than in those concerning with mining. In fact, seismic observations are the main source of information on the hydraulic fracture propagation. For this reason, the newest methods for modeling hydraulic fractures employ the observed seismicity to calibrate the input data (see, e.g. Cipolla *et al*.[2011] and Kresse *et al*.[2011]). Obviously, the reliability of the methods employed will notably gain when complimenting them with numerical modeling of seismic events and comparing synthetic seismicity with observations. The papers by Al-Busadi *et al*.[2005], Dobroskok and Linkov[2008] show that simulation of seismicity, accompanying hydraulic fracture propagation, can be efficiently performed.

Scope and Structure of the Paper

The main objective of the paper is to present the modern theory of joined modeling of mechanical state and seismicity in such a form, which provides easy implementation in a computer code of a conventional numerical method (BEM, FEM, FDM, DEM and the like). The paper also aims to:

1) Distinctly outline the fundamental issues, which stay the same when considering a wide variety of applications.

2) Point out flexible elements, which may vary depending on a particular problem and/or available computational facilities.

The exposition takes into account the mentioned tendency to carry out joined modeling in real time. It is accompanied with examples.

The structure of the papers is as follows. Firstly, we consider fundamentals of modeling a single event. This involves concepts of instability in the form of a jump, softening behavior, elastic energy release, elastic rigidity of rock near a flaw, seismic energy, seismic moment and seismic shear.

Then we consider the time effects of two kinds: those governed by processes external to the sources of events (for instance, mining steps) and those, which are defined by processes in the source of an event. The first group is the same as in conventional calculations of stresses. The second is specific and it leads us to the Elasticity-Softening-Creep (ESC) model as the simplest model capable to serve for modeling both seismic and aseismic events and intervals between the events.

Having the background for modeling a single event, we follow the line by Salamon[1993] of random seeding crack-like flaws in the rock mass and checking their stability under current stresses. Special attention is paid to proper prescribing the values and statistical distributions of geometrical and mechanical properties of seeded flaws.

With these prerequisites, we come to the general structure of a computer code for simulation of seismic and aseismic events. It appears that it is sufficient to compliment a conventional code with a set of quite general 'seismic' subroutines, which may be used in diverse computational environments. The discussion of subroutines, serving for processing the output data, is accompanied by examples of various applications. Brief summary concludes the exposition.

MODELING OF A SINGLE SEISMIC EVENT

Seismicity is a sequence of many individual events. Therefore, to simulate seismicity we need to clearly understand and properly model a single event. Having a tool for such modeling, it becomes possible to randomly generate parameters, defining an event, and to obtain statistical collection of events called synthetic seismicity.

Instability in a Form of a Jump

The essence of a seismic event is a jump from one equilibrium state to another with release of elastic energy. The excess of the elastic energy released in a jump over the energy consumption manifests itself through elastic waves, registered in (micro)seismic observations. Although wave receivers are located at a distance from the source, seismograms contain important information on the source such as its location, magnitude, seismic moment, etc. (see, e.g. Aki and Richards[2002], Gibowicz and Kijko[1994], Mendecki[1997] and Rice[1980]). These seismological data obtained at a distance from the source may be compared with that provided by an analysis of the jump in the source itself. Here we focus on such an analysis.

From the mechanical point of view, a *jump* is a form of *instability* with elastic energy excess transformed into kinetic energy of waves. Jumps occur in rock at different scales. In a loaded specimen, they occur on the level of microcracks and appear as acoustic emission. It may serve to validate modeling of seismic events under known conditions of loading. In oil and gas production, jumps appear as microseismicity around a borehole or propagating front of a hydraulic fracture. In a mine, we have a larger scale: there emerge not only microseismic events but also large dangerous jumps, rockbursts. Their magnitude in the Righter scale may reach two. Moreover, in the earth crust the length and magnitude scales are much greater; an event may appear as an earthquake. The magnitude may reach eight.

Despite the length scale changes nine orders (from micro meters to kilometres) the essence of a single event is the same: it is the dynamic (with the energy excess) instability. Consequently, proper modeling of a single event requires the study of instability and it refers to events on a wide range of scales.

Equilibrium, Stability and Instability

The theoretical canvas of studying instability in mechanics is common. Firstly, we need to find a current state. To this end, the equations of continuum mechanics for a small volume of a medium, associated with a mathematic point, are used. They include:

- Dynamic or static equations of motion (equilibrium), which are actually the Newton's second law, specified for a point of continuum.
- Kinematics equations, defining changes in mutual positions between closely located points of the medium.
- Constitutive equations for a *volume* element, which connect dynamic quantities of the first group with geometric quantities of the second.

This yields a complete system of partial differential equations (PDE), defined at points of a considered region of the medium. It is solved under prescribed initial, contact and boundary conditions to distinguish the particular solution of the PDE, corresponding to a particular problem, from the general solution.

In *static* problems, which are of prime interest to our theme, there is no need in initial conditions: we use only contact and boundary conditions. The contact conditions include constitutive equations for a *contact* element. (In the simplest case of a perfect contact, the constitutive equations express continuity of tractions and displacements through the contact).

Suppose we have found the solution of a problem and know the equilibrium state. Now we want to know if the state is stable or unstable.

A rigorous analysis of stability requires strict definitions of what is assumed to be a stable or unstable state. Naturally, the definition differs in different problems. Still, the general feature is that instability is always induced by some source(s) of non-linearity. The problem of stability does not exist for a linear system. Thus we need to inspect the possible sources of nonlinearity.

For a massive body of hard rock, in contrast with slender bodies, we may neglect non-linear terms in equilibrium and kinematics equations. Thus the only candidates to be the sources of instability remain non-linear constitutive equations for volume or/and contact elements. These equations are obtained in physical experiments with rock volumes and contacts.

Figure 2 presents typical non-linear diagrams for a *volume* element obtained by using a rigid testing machine.

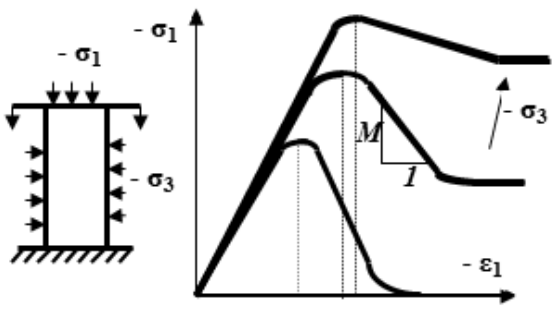

Figure 2. Complete diagrams for a volume element

Of importance is that the diagrams have descending parts, corresponding to so-called *softening* behaviour. As known from the pioneering work by Cook[1965b], under some conditions, softening becomes the source of

instability with the energy excess transformed into kinetic energy of fragments of fractured rock. Note that from the plasticity theory (e.g. Kachanov[2004]), we know that such kind of instability cannot occur for linear elasticity and hardening that is for deformation on ascending parts of diagrams.

Similarly Figure 3 presents typical non-linear shear traction-shear displacement discontinuity (DD) diagrams for a contact (surface) element. They also have descending (softening) parts. Again they may cause dynamic instability (see, e.g. Linkov[1994]).

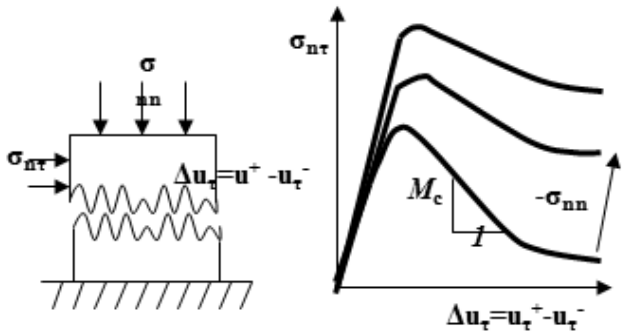

Figure 3. Complete diagrams for a contact element

Now we need to decide which of the two types of softening or both of them should be taken into account when modeling a seismic event? Actually, modern numerical techniques may account for the both types. Still the surface type looks dominating as concerns with seismicity in hard rock, at least. As wrote Napier[2001]: "*The fundamental 'building block' of material failure can then be considered to be a 'crack element' rather than a 'particle'*". Furthermore, even volumetric softening of a pillar may be modeled by using the dependence between average displacements of its boundaries and average tractions on them (see, e.g. Linkov[1994]). Thus in the problem considered, it is reasonable to focus on surface (contact) softening.

Constitutive Equations for Contact Interaction

Consider an element of rock surfaces in contact. Denote n the normal to the element, σ^+ the traction vector on that side of the contact, with respect to which the normal is outward, u^+ is the vector of displacement on this side; σ^- and u^- the traction and displacement on the opposite side (Figure 4).

Commonly, in problems involving contact instabilities, the contact is either not filled or it is filled with a material softer than embedding rock. Then we may neglect bending of a contact layer. This yields that (i) the contact interaction is characterized by the DD:

$$\Delta u = u^+ - u^-, \tag{2.1}$$

rather than by the average displacement $1/2(u^+ + u^-)$ and (ii) the traction is continuous through the contact:

$$\sigma^+ = \sigma^- = \sigma. \tag{2.2}$$

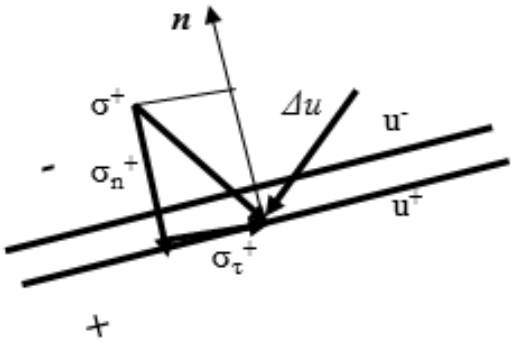

Figure 4. Traction and DD vectors on a contact

Therefore, the contact interaction is characterized by components of the vectors σ and Δu. In the component form, the vector Equation (2.2) in 3D presents three scalar equations. Three other needed equations express the dependence between the traction and DD vectors: $\sigma = F(\Delta u)$. For irreversible deformations at a contact, this dependence should be incremental, connecting increments of the tractions with increments of the DD in a way similar to plasticity theory. Quite general equations of this type may be found elsewhere (e.g. Linkov[1994]). However, having in mind that the properties of a surface are uncertain and difficult to find, using a general description looks impractical. It is reasonable to employ as simple description as possible to shorten the list of uncertain parameters. For our purpose, we shall use the following simplifications.

1) A flaw (crack), on which an event may occur, is closed if the traction does not reach the tensile strength c_{0n} or the initial shear strength $\sigma_{\tau C}$. For simplicity, the initial shear strength is prescribed by the Coulomb's law:

$$\sigma_\tau = \sigma_{\tau C} = c_{0\tau} + (-\sigma_n)\tan\rho, \tag{2.3}$$

where σ_τ is the shear component of the traction, $c_{0\tau}$ is the initial cohesion, ρ is the surface friction angle. For illustrative purposes we assume that the shear traction vector is directed along a local coordinate axis in the plane of shear; thus *we assume σ_τ positive*. Then the *shear DD is negative*, and we shall use $-\Delta u_\tau$ to have a positive value. A compressive normal traction, like compressive stresses, is assumed negative.

Thus we have:

$$\Delta u = 0, \qquad \text{if} \quad \sigma_n < c_{0n} \quad \text{and} \quad \sigma_\tau < \sigma_{\tau C}. \tag{2.4}$$

2) When the traction reaches a limit value, there DD occur.

For the *tensile mode* $(\sigma_n \ge c_{0n})$, the DD are defined by the condition that the traction on an open crack becomes zero:

$$\sigma = 0. \tag{2.5}$$

For the *shear mode* $(\sigma_\tau \geq \sigma_{\tau C})$, the DD are defined in accordance with the piece-wise linear diagrams with descending parts shown in Figure 5:

$$\sigma_\tau = \begin{cases} \sigma_{\tau C} - M_c(-\Delta u_\tau) & -\Delta u_\tau < \Delta u_* \\ \sigma_{\tau C} - (c_{0\tau} - c_{*\tau}) & -\Delta u_\tau \geq \Delta u_* \end{cases}, \qquad (2.6)$$

where M_c is the shear softening modulus, $\Delta u_* = (c_{0\tau} - c_{*\tau})/M_c$ is the shear DD, corresponding to reaching the residual cohesion $c_{*\tau}$.

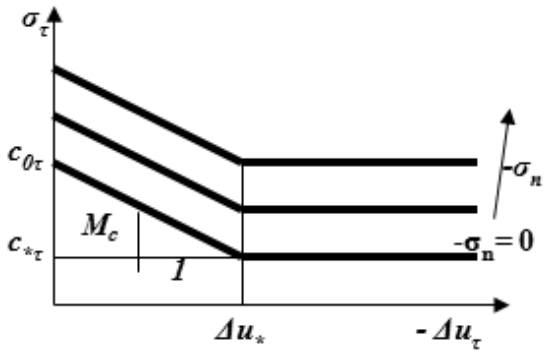

Figure 5. Simplest diagrams for a shear softening contact

The normal DD Δu_n for the shear mode may be prescribes as

$$-\Delta u_n = -\Delta u_\tau \tan\psi, \qquad (2.7)$$

where ψ is the dilation angle. The minus sign in front of Δu_n serves to have a positive value. Recall that we assume Δu_τ to be negative and that under the accepted definition (2.1) of DD, a DD, corresponding to opening, is negative (see Figure 4). Commonly, we may neglect the dilation; then $\Delta u_n = 0$ for the shear mode.

Equations (2.1) – (2.7) completely define the properties of a contact element. The dependence (2.6) accounts for softening what serves for modeling dynamic instability.

Softening Contact in Rock. Instability

We explain dynamic instability, caused by contact softening, by considering the simplest system shown in Figure 6a. It presents a specimen with the length l and the elasticity modulus E. The specimen is cut under the angle α and it is loaded in a rigid testing machine. Two elastic parts of the specimen interact along the contact surface, for which shear deformation occurs in accordance with the diagram shown by the solid line in Figure 6b.

The elastic parts represent an external (with respect to the softening contact) system, which accumulates elastic energy. Continuous deformation of the contact may become impossible when its shear strength is reached and softening starts. It is easy to show (Linkov[1994]) that unique solution of the problem exists only when the softening modulus M_c is less that the shear rigidity K_S of the external system:

$$M_c < K_S. \qquad (2.8)$$

Herein, the shear rigidity is evaluated per unit contact area; in the considered case $K_S = (E/l)\sin\alpha\cos^2\alpha$.

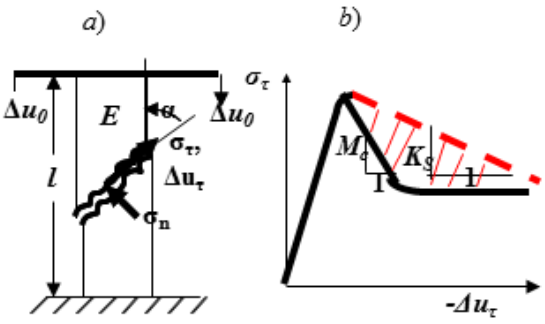

Figure 6. Example of instability caused by contact softening

If the inequality (2.8) is not satisfied, then we have either infinite number of solutions, corresponding to any point of the descending part when $M_c = K_S$, or a jump to the residual strength when $M_c > K_S$. The dashed line in Figure 6b shows the corresponding mutual deformation of elastic parts. The hatched area shows the energy excess (per unit area), accompanying the jump from the initial shear strength to its residual value. Thus when $M_c > K_S$, we have dynamic instability.

The case $M_c = K_S$ is intermediate between stable deformation and dynamic jump. In this case, the elastic energy release equals to the energy consumption at the softening interface. Although the energy excess is zero, we shall relate this case to instability because the solution losses uniqueness and whatever small exceeding of M_c over K_S results in a dynamic event. Thus if the shear strength is reached, the state is unstable and jump to the residual strength occurs when

$$M_c \geq K_S. \qquad (2.9)$$

Otherwise, the state is stable.

From the general theory of dynamic instability (Linkov[1987], see also Linkov[1994, 1997]) it follows that applicability of the simple conditions of stability (2.8) and instability (2.9) in terms of the elastic rigidity and the softening modulus is quite limited. In general, we need to use conditions in terms of energy excess on virtual displacements. Nevertheless, the simplicity of the conditions (2.8), (2.9) is very attractive. It appears that it is possible to apply them to modeling seismic events. Specifically, they are applicable to crack-like flaws in elastic rock when the shear rigidity K_S of the external system is properly defined.

Rigidity of a Crack-like Flaw

Consider, for certainty, a rectangular crack-like flaw with the minimal size a and the other side b $(b \geq a)$ in

elastic rocks with the elasticity modulus E and the Poisson's ratio ν (Figure 7). We use the local coordinate system with the axis x_1 normal to the flaw plane, x_2 and x_3 in the plane. The x_2-axis is directed along the long side of the rectangle, the x_3-axis is along the short side. The flaw sizes are small as compared with the sizes of openings, faults and other structural elements of a considered region. Then the total influence of these disturbing factors and stresses at infinity is incorporated in the total traction t_Σ, induced at the location of the flaw on its surface.

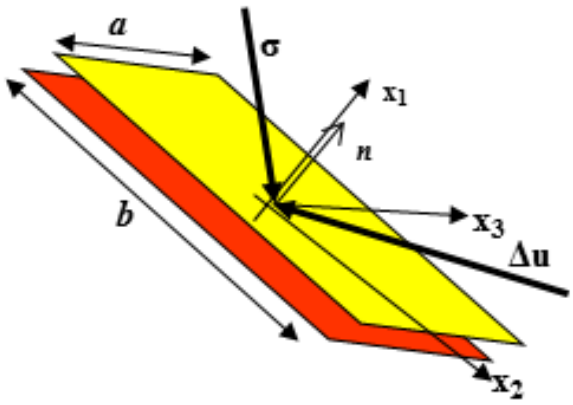

Figure 7. A rectangular flaw in elastic rock

It is easy to solve numerically a 3D problem for a plane crack of an arbitrary configuration in an infinite elastic region under prescribed traction at the crack surface (e.g. Linkov *et al.*[1997]). From the solution we can find the dependence between the average traction vector σ and the average DD vector Δu:

$$\sigma = K\,\Delta u + t_\Sigma\,, \tag{2.10}$$

where K is a matrix with known coefficients; it has the meaning of average (per unit area) rigidity matrix. In particular, for a rectangular crack in isotropic rock, by symmetry, the rigidity matrix is diagonal. Its diagonal coefficients K_1, K_2 and K_3 may be written as:

$$K_i = \frac{E}{1-\nu^2}\frac{k_i}{a}\,, \tag{2.11}$$

where the dimensionless coefficients k_i $(i = 1, 2, 3)$ depend on the ratio b/a; besides the coefficients k_2 and k_3 depend on the Poisson's ratio.

Figure 8 presents the graphs of the coefficients k_i as functions of b/a for the Poisson's ratio $\nu = 0.25$ (Linkov[2006]). Note that in the limiting case of a plane-strain problem $(b/a \to \infty)$, the coefficients found analytically are: $k_1 = 2/\pi$, $k_2 = 2/\pi$, $k_3 = 2(1-\nu)/\pi$. From calculations it follows that to the accuracy of 3% the plain-strain conditions are acceptable when $b/a = 4$. This implies that the coefficients k_2 and k_3 differ by the factor $1-\nu$ at most. Therefore, for simplicity, we may use their mean value $k_S = (k_2 + k_3)/2$, which becomes the only characteristic of shear rigidity. (The bold line in Figure 8 gives the dependence of k_S on the ratio b/a). Then (2.11) becomes:

$$K_1 = \frac{E}{1-\nu^2}\frac{k_1}{a}\,,\ K_S = K_2 = K_3 = \frac{E}{1-\nu^2}\frac{k_S}{a}\,. \tag{2.12}$$

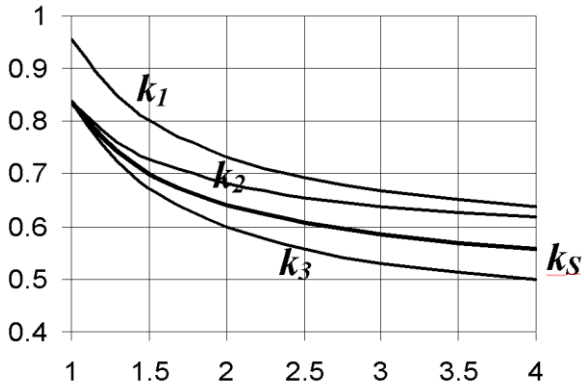

Figure 8. Rigidities as functions of *b/a*

In view of (2.12), we may write the dependence (2.10) between the average DD and average tractions in terms of separated normal σ_n, Δu_n and shear σ_τ, Δu_τ components:

$$\sigma_n = K_1\Delta u_n + t_{\Sigma n}\,,\ \sigma_\tau = K_S\,\Delta u_\tau + t_{\Sigma\tau}\,. \tag{2.13}$$

Equations (2.13) notably simplify analysis of the system "flaw – embedding rock". The *unified shear rigidity* K_S makes the rectangular flaw isotropic in its response to shear, like it is for a circular flaw. By employing this simplification, from now on, we shall assume the local coordinate x_2 directed along the shear traction.

Comment. The actual configuration of flaws in rock mass is uncertain. Thus there is no sense to distinguish between the shear rigidities K_2 and K_3 and to exactly specify the Poisson's ratio. Moreover, as the shear rigidity K_S is compared with the shear softening modulus M_c, which is even more uncertain, it is enough to use rough estimations. In particular, since the shear rigidity changes only 1.6-fold when the rectangle changes from a square $(b = a)$ to an infinite strip $(b/a = \infty)$, it is possible to set $b = a$. Then for $\nu = 0.25$, the rigidities are:

$$K_1 = 1.0\frac{E}{a}\,,\ K_S = 0.9\frac{E}{a}\,. \tag{2.14}$$

Note that the analytical solution for a circle of the radius $R = a/2$, yields the normal rigidity $K_1 = 0.95E/a$; the difference with the first of (2.14) is only 5%. Thus the configuration of a flaw does not influence the rigidity significantly. Roughly, the rigidity is defined by the minimal size of a flaw. Using a circular flaw simplifies also input data and estimations of the energy release. For these reasons, Salamon[1993] seeded circular flaws.

Equilibrium and Instability of a Crack-like Flaw in Rock

We are in a position to obtain an approximate solution for a softening crack-like flaw by equating the tractions and DD on its surface to those of elastic rock. Before the tensile or shear strength is reached $(t_{\Sigma n} < c_{0n},\ t_{\Sigma\tau} < \sigma_{\tau C})$, Equations (2.4) and (2.10) yield the obvious result:

$$\sigma = t_{\Sigma}\ .$$

After the tensile strength is reached $(t_{\Sigma n} \geq c_{0n})$, Equations (2.5) and (2.10) give:

$$-\Delta u = K^{-1} t_{\Sigma}\ . \qquad (2.15)$$

At last, if the shear strength is reached $(t_{\Sigma\tau} \geq \sigma_{\tau C})$, joining the first of (2.6) and the second of (2.13) gives the system, defining the shear DD under softening:

$$\sigma_\tau = \sigma_{\tau C} - M_c(-\Delta u_\tau)\ ,\ \sigma_\tau = K_S\,\Delta u_\tau + t_{\Sigma\tau}\ .$$

Its solution is:

$$-\Delta u_\tau = \frac{t_{\Sigma\tau} - \sigma_{\tau C}}{K_S - M_c}\ . \qquad (2.16)$$

Recall that by the accepted agreement on signs, for a physically significant solution, it should be $-\Delta u_\tau > 0$. Since the numerator in (2.16) is non-negative, this implies that a continuous solution exists only under the condition of (2.8) form: $M_c < K_S$. If $M_c \geq K_S$, there is no continuous solution: the system jumps to the state corresponding to the residual strength. We see that the condition (2.9) is the condition of dynamic instability for a flaw in elastic rock.

For the final state after the jump, the second line in (2.6) and the second Equation in (2.13) yield:

$$-\Delta u_\tau = \frac{t_{\Sigma\tau} - \sigma_{\tau C} + (c_{0\tau} - c_{*\tau})}{K_S}\ . \qquad (2.17)$$

Note that the r. h. s. in (2.17) is positive.

Comment. Recall that the solutions (2.16), (2.17) are approximate because we have used tractions and DD averaged over a flaw. It is of interest to estimate the accuracy of such an approach. It can be done by using the results of the exact solution to the plain-strain problem for a straight shear-softening crack of the length a in elastic rock (Belov and Linkov[1995]). From inspecting dimensions, it is obvious that the condition of dynamic instability has the form (2.9). The value of the rigidity, corresponding to the exact solution, is $K_S = 0.675\frac{E}{1-\nu^2}\frac{1}{a}$. Its comparison with the approximate value $K_S = \frac{2}{\pi}\frac{E}{1-\nu^2}\frac{1}{a}$, obtained by averaging, shows that the error is 9.3%. Such an error looks acceptable when modeling a seismic event.

Seismic Characteristics of a Single Event

Consider a flaw with the normal n in rock (Figure 7). Suppose that the tractions σ_n and σ_τ are such that the shear strength is reached. Then the flaw may experience softening in accordance with a diagram in Figure 5, corresponding to the current normal traction $\sigma_n = t_{\Sigma n}$. This diagram is shown by solid line in Figure 9.

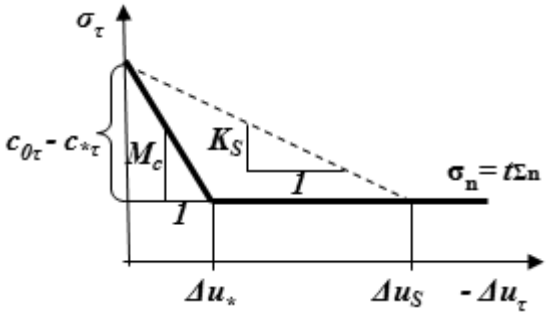

Figure 9. Diagrams of softening element and external system (embedding rock)

We are interested in characteristics of the jump occurring when the instability condition,

$$M_c \geq K_S\ ,$$

is met. Then the deformation of rock surfaces follows the diagram shown by the dashed line in Figure 9. The area between the diagrams represents the energy excess per unit area. Therefore, for the whole flaw area, equal to ab, the total elastic *energy excess* is:

$$W = \frac{1}{2}\frac{(c_{0\tau} - c_{*\tau})^2}{K_S}\left(1 - \frac{K_S}{M_c}\right)ab\ . \qquad (2.18)$$

Note that the total elastic *energy release* is

$$W_r = \frac{1}{2}\frac{(c_{0\tau} - c_{*\tau})^2}{K_S}ab\ , \qquad (2.19)$$

while the total *energy consumption* on the softening surface is $W_C = 1/2(c_{0\tau} - c_{*\tau})^2 ab/M_c$. Introduce the seismic efficiency factor, defined in seismology as $K_{eff} = (W_r - W_C)/W_r$, so that $W = K_{eff}W_r$. Then Equation (2.18) implies that in the considered case the seismic efficiency is:

$$K_{eff} = 1 - \frac{K_S}{M_c}\ . \qquad (2.20)$$

Depending on the softening modulus it may change from the unity for ideally brittle rock, considered by Salamon[1993] $(M_C = \infty)$, to zero at the threshold of instability $M_C = K_S$.

We obtain a rough estimation of the seismic energy by using the second of Equations (2.14) for a square flaw:

$$W = 0.56\frac{(c_{0\tau} - c_{*\tau})^2}{E}a^3 K_{eff}\ . \qquad (2.21)$$

Equation (2.21) shows that the energy of an event is proportional to the *cubed* crack size a. The simple estimation (2.21) is useful in numerical simulation of seismicity. It serves for the choice of the average size of flaws, which define the average level of energy; the latter is available from seismic observations.

The seismic shear Δu_S, according Figure 9, is:

$$\Delta u_S = \frac{c_{0\tau} - c_{*\tau}}{K_S}. \qquad (2.22)$$

The tensor of seismic moment in the local coordinates of the flaw is:

$$M_{seism} = -m \begin{pmatrix} 0 & 1 & 0 \\ 1 & 0 & 0 \\ 0 & 0 & 0 \end{pmatrix}.$$

Herein, m is the magnitude, defined as usual by the equation $m = \mu \Delta u_S S$, where μ is the shear modulus $2\mu = E(1+\nu)$, S is the flaw area $(S = ab)$. (Recall that we have assumed the local coordinate x_2 directed along the shear traction, so that the shear DD has the direction opposite to x_2 what explains the minus sign in front of m). One nodal plane of an event is normal to the local axis x_1, another is normal to x_2.

Usual tensor transformation gives the tensor of seismic moment in a global system of coordinates. For brevity, the value m is also called the seismic moment when there might be no confusion.

Using (2.22) yields:

$$m = \mu \frac{c_{0\tau} - c_{*\tau}}{K_S} ab. \qquad (2.23)$$

From (2.19) and (2.23), it follows that the energy release is proportional to the moment m:

$$W_r = \frac{c_{0\tau} - c_{*\tau}}{2\mu} m.$$

The energy excess differs only by the seismic efficiency factor:

$$W_e = \frac{c_{0\tau} - c_{*\tau}}{2\mu} m K_{eff}.$$

Therefore, in rough estimations, assuming the seismic efficiency constant, the energy excess is proportional to the seismic moment.

Summary for Modeling a Single Seismic Event

We have seen that the essence of a seismic event is instability in the form of a jump. It occurs when the elastic energy release exceeds the energy consumption for softening deformation of a flaw. Therefore, when modeling a single event we need to account for:

1) Elasticity, which provides the source of energy.

2) Softening, which defines the energy consumption.

Thus,

Elasticity + Softening → Single seismic event

This implies that when seeding many flaws, at which seismic events may occur, the minimal input data for a flaw are:

1) Its location (three global coordinates of the flaw center).

2) Orientation of the flaw plane (two coordinates of the unit normal to the plane; and, for a rectangular flaw, orientation of one of the sides in the plane).

3) The size(s) of the flaw (two lengths of a rectangle, or one size for a square or circle).

4) Mechanical properties of the flaw: its tensile c_{0n} and initial shear $c_{0\tau}$ strength, friction angle ρ, residual cohesion $c_{*\tau}$, softening modulus M_c and dilation angle ψ; in simplified models, one may set $c_{0n} = 0$, $c_{*\tau} = 0$, $\psi = 0$ and/or consider ideally brittle contact $(M_c = \infty)$.

5) Elasticity modulus E and Poisson's ratio ν of rock at the location of the flaw.

The elastic properties of rock and minimal size of a flaw define the shear rigidity K_S of rock with respect to the flaw. It is found from the second of Equations (2.12) and Figure 8 for a rectangular flaw, or from the second of Equations (2.14) for a square or circular flaw with the radius $R = a$.

The behavior of a flaw in rock depends on the tractions t_Σ induced on its surface by external stresses. The stresses are found by solving a boundary value problem for rock masses with openings, faults, inclusions, etc. under prescribed in-situ stresses. A common code of FEM, BEM, DEM and the like may serve to find the induced stresses.

A flaw is closed and it does not influence the rock state when neither tensile, nor shear strength is reached.

A flaw opens when the normal traction becomes equal or exceeds its tensile strength $(t_{\Sigma n} \ge c_{0n})$; then the flaw obtains the DD defined by (2.15).

A flaw experiences shear deformation when its shear strength is reached $(t_{\Sigma\tau} \ge \sigma_{\tau C})$. In this case, there are two options:

1) There is no seismic event if the stability condition (2.8) is met $(M_c < K_S)$. Then the shear DD is found from (2.16); the normal DD is defined by (2.7); when setting the dilation angle ψ zero, the normal DD is zero.

2) A seismic event (jump) occurs if the instability condition (2.9) is met $(M_c \ge K_S)$. Then the characteristics of the event (energy release, energy excess, seismic

efficiency, seismic shear, seismic moment, etc.) are found by using Equations (2.18) – (2.23).

TIME EFFECTS

Multiple Events: Seismicity

Time effects are obviously present in rock. "*The first law of rock mechanics is that holes tend to close up*" (saying of "wise old engineer" quoted by van der Merwe[1995]). As concerns with seismic events, they are distributed in time; obviously time effects control intervals between individual events. They lead also to aseismic deformations. Thus to consider many seismic events and to include aseismic events, we need to compliment the two discussed fundamental factors (elasticity and softening) with time. A multiplicity of seismic events is called seismicity. Therefore,

Elasticity + Softening + Time → Seismicity

For events of small magnitude, the term microseismicity is commonly used; dynamic events in a loaded specimen are called acoustic emission. We assume these terms equivalent.

External Time

It looks reasonable to distinguish two types of time processes:

1) Those which run out of the source of an event and its close vicinity.

2) Those which occur in the source and its close neighbourhood.

The first group of processes is *external*, while the second is *internal* with respect to an event.

Figure 10 presents examples of processes controlled by external time. They include a specimen loaded with stresses, which change in time in accordance with a prescribed loading path (Figure 10*a*); mining with changes of geometry planned by an engineer (Figure 10*b*). In these two cases the time is just a parameter defining changes in boundary conditions. The other two examples refer to oil (gas, heat) production (Figure 10*c*), where changes in the stressed state are defined by transient processes of fluid flow, and propagation of a hydraulic fracture (Figure 10*d*), which changes the stresses around it.

Various conventional codes of FEM, BEM, DEM, etc. may serve to numerically trace the change of stresses in the external time. We assume that a numerical code to simulate these changes is available. From now on we focus on the 'internal time'.

Internal Time. Elasticity-Softening-Creep (ESC) Model

There is obvious evidence of internal time present in seismicity: after a strong excitation of rock, such as an earthquake, or rockburst, or blast, a cascade of seismic events occurs during some interval of time. The events cease in time approximately exponentially, what in seismology is called the Omori's law. The questions are: how to account for the internal time in the simplest way and how to model aseismic events?

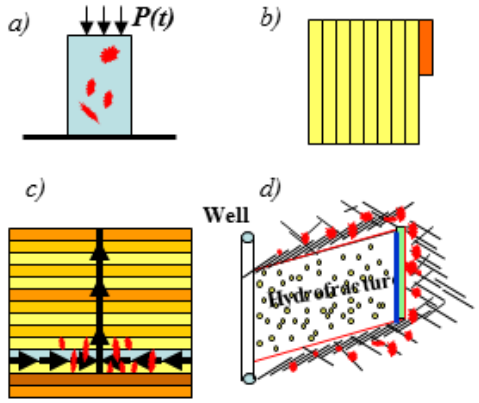

Figure 10. Examples of processes running in 'external' time

We may follow the common path of solid mechanics to get an answer. As known, the simplest description, explicitly accounting for the time, is the Newton's viscosity law, which linearly connects a force (stress) with a kinematic quantity (velocity, strain rate, DD). In schemes, presenting model behavior, it is shown by a dash-pot (Figure 11*a*).

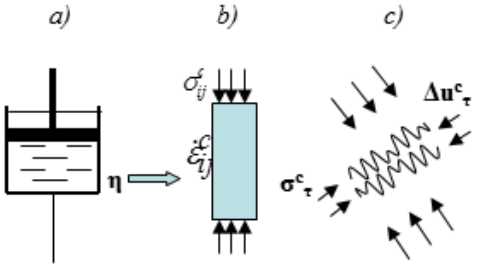

Figure 11. Using a dash-pot (*a*) to simulate viscous deformation of a volume (*b*) or surface (*c*) element

In constitutive equations for a volume element (Figure 11*b*), the dependence between a time-dependent part of the stress $\sigma_{ij}^{\ c}$ and the strain rate $\varepsilon_{ij}^{\ c}$ is $\sigma_{ij}^{\ c} = \eta\dot{\varepsilon}_{ij}^{\ c}$ with the coefficient η having the dimension of dynamic viscosity $[\eta]$ = stress/strain rate = stress·time. For a contact element (Figure 11*c*), time-depending shear traction σ_τ^c linearly depends on the velocity $\Delta\dot{u}_\tau^c$ of shear DD: $\sigma_\tau^c = \eta\Delta\dot{u}_\tau^c$ with the coefficient η having the dimension $[\eta]$ = stress/velocity = stress·time/length. The dot over a symbol denotes the derivative with respect to time.

There are numerous option for including this model into constitutive equations for embedding rock (volumes) or/and interfaces (surfaces). When choosing between them, it is reasonable to have in mind that a dash-pot responds absolutely rigidly to instant changes. Actually its *instant*

rigidity is infinite. Specifically, its reaction is absolutely rigid in a jump, which corresponds to dynamic instability associated with a seismic event. Consequently, there is *no sense to include a viscous element in parallel* with an elastic element when modeling external system, represented by external rock (Figure 12*a*). Such a system will not provide elastic energy instantly. It is also senseless to include a viscous element in parallel with a softening element modeling the behavior of a crack-like flaw (Figure 12*b*). Such a system is unable to consume energy in a jump.

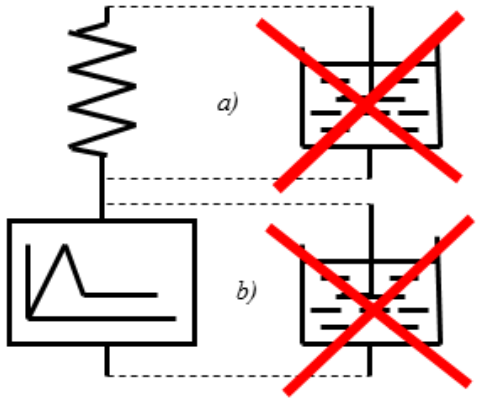

Figure 12. Schemes with parallel inclusion of a viscous element

We conclude that the reasonable way of accounting for internal time is to include a viscous element *in series* with an elastic element representing an external system (Figure 13*a*), or/and with a softening element shown in Figure 13*b*.

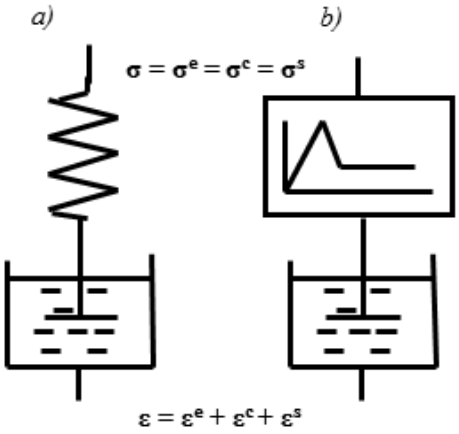

Figure 13. Schemes with inclusion of a viscous element in series

In the simplest softening element shown in Figure 5, we have neglected the elastic DD on the flaw surface. Consequently, to have a time scale, it is reasonable to use the viscous element in frames of the Kelvin-Voight model.

Then we obtain the simplest model (Figure 14), which exhibits instant softening and has a characteristic time t_r. We call this model the Elasticity-Softening-Creep (ESC) model, because it includes the *elastic* element with the rigidity E_l, *softening* element with the softening modulus M_c and viscous (*creeping*) element with the viscosity η. The *characteristic time* of the model is the retardation time:

$$t_r = \frac{\eta}{E_l}. \tag{3.1}$$

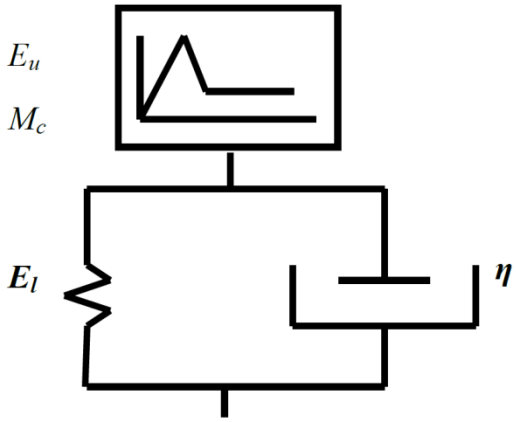

Figure 14. Elasticity-Softening-Creep model

The instant reaction of the model is that of the softening element with the *instant softening modulus* M_c. The long term reaction is that of a softening element with the *long-term softening modulus* M_∞, defined by equation:

$$\frac{1}{M_\infty} = \frac{1}{M_c} - \frac{1}{E_l}. \tag{3.2}$$

The ESC-model is the simplest extension of the standard linear body. It reduces to the standard body when excluding softening of the upper element in Figure 14, so that it becomes elastic. Below we shall use the opposite option and neglect elastic deformation of the upper element. Surely, non-Newtonian viscous element may be used when appropriate.

ESC-model, being not much more complicated than models used to the date, it provides significant advantages. It allows us to account for rock brittleness, to distinguish between stable and unstable states, to evaluate energy consumption and to follow damping or accelerating aseismic deformations.

Constitutive Equations for ESC-Model

We shall use the simplified diagrams of Figure 5 and their analytical form (2.6). The corresponding ESC-model is shown in Figure 15.

The properties of the model are as follows. Until the tensile or shear strength is reached, we assume that a flaw is closed and DD at its surface are zero. If the tensile strength is reached, the reaction is instant, thus the flaw opens and the traction turns to zero (Equation 2.5). If the shear strength is reached, then the upper element of the

ESC-model behaves in accordance with Equations (2.6). We rewrite them with the subscript ‘u’ at the shear DD to mark that the DD refer to the upper element in Figure 15:

$$\sigma_\tau = \begin{cases} \sigma_{\tau C} - M_c(-\Delta u_{\tau u}) & -\Delta u_{\tau u} < \Delta u_* \\ \sigma_{\tau C} - (c_{0\tau} - c_{*\tau}) & -\Delta u_{\tau u} \geq \Delta u_* \end{cases}. \qquad (3.3)$$

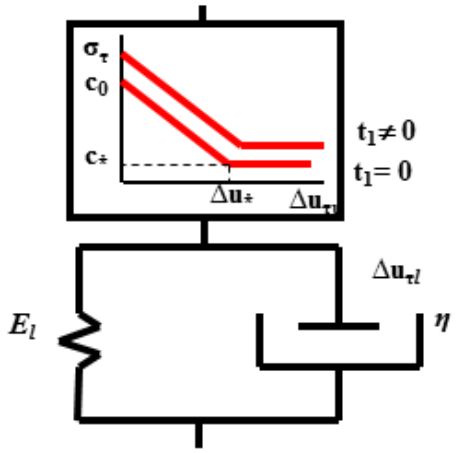

Figure 15. ESC-model (no elastic DD prior softening)

For the lower Kelvin-Voight element, we have:

$$\sigma_\tau = E_l(-\Delta u_{\tau l}) + \eta(-\Delta \dot{u}_{\tau l}), \qquad (3.4)$$

where the subscript l marks that the DD refers to the lower element. The traction is the same in the upper and lower element because they are joined in series. For the same reason, the total DD is the sum:

$$\sigma_\tau = E_l(-\Delta u_{\tau l}) + \eta(-\Delta \dot{u}_{\tau l}). \qquad (3.5)$$

The total normal DD may correspond to dilation in accordance with (2.7).

Joined System of ESC-Surface Element and Rock

We join Equations (2.13) of the external system with Equations (3.3) – (3.5) for a flaw described by the ESC-model. If neither tensile nor shear strength is reached, the flaw is closed; its DD are zero. If the tensile strength is reached, the DD are defined by Equation (2.15). If the shear strength is reached $(t_{\Sigma\tau} \geq \sigma_{\tau C})$, the joined system yields the ordinary differential equation (ODE):

$$\frac{d(-\Delta u_\tau)}{dt} + \frac{\alpha}{t_r}(-\Delta u_\tau) = \frac{\beta}{t_r}(t_{\Sigma\tau} - \sigma_{\tau C}), \qquad (3.6)$$

where t_r is the retardation time defined by (3.1),

$$\alpha = \frac{K_S / M_\infty - 1}{K_S / M_c - 1}, \ \beta = \frac{1/M_\infty}{K_S / M_c - 1}, \qquad (3.7)$$

M_∞ is the long-term softening modulus defined by (3.2); note that (3.2) implies inequality $M_\infty > M_c$. When deriving the ODE (3.6) we neglected the viscous deformation, which occurred long before the current time, and the time derivative of the induced traction. The agreements on the signs of shear DD and shear traction are those accepted above.

The ODE (3.6) is solved under the initial condition $\Delta u_\tau(t_0) = 0$, where t_0 is the moment when the shear strength is exceeded. We shall not write down the obvious solution. Rather we discuss the general solution of a homogeneous ODE, corresponding to (3.6), because it defines general features of the mechanical system. The general solution, including an arbitrary constant C, is:

$$\Delta u_g(t) = C \exp\left(-\alpha \frac{t}{t_r}\right). \qquad (3.8)$$

From (3.8) it is clear that a solution exponentially grows (decays) when $\alpha < 0$ $(\alpha > 0)$. The sign of α depends on the signs of numerator and denominator in the first of (3.7). This implies that there are three types of shear motion depending on particular values of K_S, M_c and M_∞:

1) *Instant instability* (jump) occurs when $M_c \geq K_S$.

Then we have a seismic event with characteristics discussed in the previous subsection.

Otherwise, the state is stable ($M_c < K_S$). In this case, the deformation occurs in aseismic (without energy excess) form. Although it is continuous in time, there appear two additional options (we do not consider the exclusive case $M_c = K_S$, which is not of practical interest):

2) *Decaying* aseismic motion occurs if $M_\infty < K_S$.

3) *Accelerating* aseismic motion occurs if $M_\infty > K_S$.

We see that the ESC-model describes both seismic and aseismic events. For the latter, the motion may be very fast when the instant softening modulus M_c is close to the rigidity K_S: $-\alpha \to \infty$, when $M_c \to K_S$. This explains why intervals between observed seismic events are different; the difference may be of several orders. The fast aseismic motion explains also so-called silent earthquakes (see, e.g. Linder *et al.*[1996], Dragert *et al.*[2001] and Kawasaki[2004]).

From the analysis it appears that, actually, we need to prescribe only three parameters t_r, M_c / K_S and M_∞ / K_S to model the deformation of a flaw after its initiation by external shear traction.

Aseismic Behavior and Characteristics of a Single Aseismic Event

We have seen that aseismic motion at flaw surfaces occurs when the stability condition $M_c < K_S$ is met. The motion runs with acceleration if the long-term modulus exceeds the rock rigidity $(M_\infty > K_S)$. Otherwise, it decays in time. In the both cases, if the residual shear strength is reached in the course of motion, we have for the final shear DD:

$$\Delta u_f = \frac{t_{\Sigma\tau} - \sigma_{\tau C} + c_{0\tau} - c_{*\tau}}{K_S} . \qquad (3.9)$$

The time t_f of reaching the residual shear strength is:

$$t_f = -\frac{t_r}{\alpha} \ln\left[\frac{1 - M_c / K_S}{1 - M_c / M_\infty}\left(1 - \frac{\Delta u_{*\infty}}{\Delta u_\infty}\right)\right], \qquad (3.10)$$

where $\Delta u_\infty = (t_{\Sigma\tau} - \sigma_{\tau C})/(K_S - M_\infty)$, $\Delta u_{*\infty} = \Delta u_* M_c / M_\infty$, $\Delta u_* = (c_{0\tau} - c_{*\tau}) / M_c$. Equations (3.9) and (3.10) refer to both accelerating and decaying motion.

MODELING OF SEISMICITY. INPUT DATA

General Considerations

With the ESC-model, we can simulate a single seismic or aseismic event arising at a flaw with prescribed position of its center and orientation of its plane. It is assumed that there is a computer code, which provides stresses at the flaw location as a function of external time. Then if at some instant the tensile or shear strength is reached, we have an event (seismic or aseismic) with known time, location, orientation, seismic and aseismic DD and other characteristics discussed above.

Obviously, when having many flaws, we simulate events distributed in space and time. Therefore, to model seismicity, it is sufficient to seed a set of flaws in an area of interest and to check the state of each of them on steps of external time.

There are two comments to this general scheme. Firstly, imagine that the flaws are seeded in a natural state of rock, which is not disturbed by mining or oil (gas) production. We may expect that in situ tractions at some of the flaws exceed the shear strength. Then, in accordance with the discussion, there should be DD at such flaws. However, these DD may be referred to times long before the current time. Clearly these DD should be excluded from the totality of seeded events. In a computer code, it has to be done by a special subroutine checking seeded flaws under in situ stresses and excluding those initiated by these stresses. We shall call this subroutine "ExclusInSitu".

Secondly, an event arising at a flaw on a time step leads to DD on the flaw. The DD notably change the stresses around the flaw. The change of stresses may be strong enough to initiate some of the neighbouring flaws. Each of the initiated flaws, in its turn, experiences DD, influences its neighbours and may initiate new flaws. And so on, till new flaws are initiated. In this way, there may arise chains of seismic and aseismic events.

Obviously, if the density of flaws is small, they practically do not interact. Then there are no chains of the type. On the other hand, if the density is too high, there arises a *chain reaction*, involving practically all the flaws. The case intermediate between the two is of major interest for simulation of seismicity. In this case, we may expect that it will be possible to model the dependence of Omori type. Therefore, it is of value to find the range of flaw density, in which a chain reaction does not arise while the interaction of flaws is sufficient to produce successive cascades of events. Below we shall define the range.

Deterministic Input Data

We have assumed that a computer code is available for calculating stresses at each point of a region as functions of the external time. The input data of the code commonly contain:

1) Initial geometry of a problem; specifically, for a mining problem, we prescribe the depth, dip angle, strike angle, contours of pillars and openings.

2) Physical properties of a medium.

3) In situ stresses.

4) Some additional information for a particular problem, such as pumping rate and fluid viscosity for hydraulic fracturing, pore pressure and permeability of rock for oil (gas, heat) production, etc.

All these data are prescribed in the same way as in cases when a code is used without simulation of seismicity. Normally these data are *deterministic*.

The influence of the external time is also deterministic. Specifically, in mining problems, we plan the change of mining geometry in time; in hydraulic fracturing, we follow the fracture propagation and the change of the net-pressure in time steps of calculations.

Briefly, we assume deterministic all what concerns with the performance of a conventional code when there is no simulation of seismicity. The following discussion entirely refers to parameters specific for modeling seismic and aseismic events. They include geometric input data on positions and orientations of randomly seeded flaws, data on flaw sizes and density, data on mechanical properties of flaws. In the next subsection we specify prescribing these data. In a computer code, a special subroutine produces these data. We call it "FlawInput".

Input Data on Position and Orientation of Seeded Flaws

We seed flaws in a parallelepiped with the sides parallel to the global coordinates, with the sizes X_1, X_2 X_3 and volume $V = X_1 X_2 X_3$. The sizes notably (three- to five-fold) exceed those of the region of interest, where we want to model seismic and aseismic events.

The *uniform* random distribution is used for:

1) Three coordinates of the flaw center, changing in the intervals $[-X_1/2, X_1/2]$, $[-X_2/2, X_2/2]$ and $[-X_3/2, X_3/2]$ for the global coordinates x_1, x_2 and x_3, respectively.

2) Dip angle of a flaw changing from 0 to π/2.

3) Strike angle changing from 0 to 2π.

4) Rotation angle in the dip plane, changing from 0 to π (for a rectangular flaw).

5) Ratio b/a, changing from 1 to 3 (for a rectangular flaw).

In general the total number of geometric parameters is seven. For square flaws $(a = b)$, the item (v) is not used; the number of parameters is six. For circular flaws $(a = R)$, the item (iv) is not used, as well; the number of parameters is five.

For the size a of a flaw, we use the *exponential* distribution of the probability density:

$$P(a) = \frac{1}{l}\exp\left(-\frac{a}{l}\right), \qquad (4.1)$$

where l is the average length of the smallest side. The average length l and the total number N of the flaws are prescribed as explained below.

Input Data on Mechanical Properties of Seeded Flaws

Shear rigidity K_S. Having the input data on the rock elasticity modulus and the sizes of flaws, we find the shear rigidity from the second Equation (2.12) or (2.14).

Tensile strength c_{0n}. Commonly we may assume that the tensile strength is zero: $c_{0n} = 0$.

Shear strength $c_{0\tau}$, $c_{*\tau}$, ρ. The shear strength is characterized by the initial cohesion $c_{0\tau}$, residual cohesion $c_{*\tau}$ and the contact friction angle ρ. As follows from Equations (2.18), (2.19), (2.22) and (2.23), actually we need the difference $c_{0\tau} - c_{*\tau}$, rather than $c_{0\tau}$ and $c_{*\tau}$ separately. Therefore, we may set $c_{*\tau} = 0$. To reduce the number of quite uncertain parameters, like $c_{0\tau}$ and ρ, we may prescribe the latter two quantities by their average values. In particular, for hard rocks, according to Salamon[1993], the initial cohesion changes from 0.02 to 4.3 MPa with the statistically mean value $c_{0\tau} = 2.5$; the friction coefficient $\tan\rho$ changes from 0.5 to 1 with the mean friction angle $\rho = 31^0$. When high confining pressure prevents shear, the number of initiated events may be increased by decreasing the friction angle to 20° or even to 10°.

Shear softening modulus M_c. For the prescribed shear rigidity K_S, prescribing the softening modulus is equivalent to that of the ratio M_c / K_S. The latter defines the instability condition and seismic efficiency. As both M_c and K_S decrease with growing crack size, they are partly correlated. Still their ratio is a random quantity and quite uncertain. We may prescribe the ratio M_c / K_S as a sum of the determined (mean) part a_M and the random part $b_M f_M$, *uniformly* distributed on the interval $[-b_M, b_M]$:

$$\frac{M_c}{K_S} = a_M + b_M f_M, \qquad (4.2)$$

where $a_M > b_M$, f_M is a random value uniformly distributed on the interval [-1, 1]. The values of a_M and b_M in (4.2) may be prescribed by using the following considerations.

If $a_M - b_M \geq 1$, then $M_c / K_S \geq 1$; hence in accordance with the instability condition (2.9), all the modeled events will be seismic. In modeling, this choice serves to neglect aseismic events.

If $a_M + b_M < 1$, then $M_c / K_S < 1$; hence all the modeled events will be aseismic. In modeling, this choice serves to model only aseismic events.

If $|a_M - 1| < b_M$, the ratio of numbers of modeled seismic events N_S to that of aseismic events N_A is:

$$\frac{N_S}{N_A} = \frac{b_M + (a_M - 1)}{b_M - (a_M - 1)}. \qquad (4.3)$$

Thus, by an appropriate choice of a_M and b_M, one may adjust the ratio of seismic to aseismic deformation to data of observations. Note that when $a_M = 1$, Equation (4.3) implies that the number of seismic events equals to the number of aseismic events for any value of b_M.

The mean seismic efficiency of seismic events is:

$$K_{eff} = \frac{a_M + b_M - 1}{a_M + b_M + 1}. \qquad (4.4)$$

Therefore, one may choose the parameters a_M and b_M to prescribe the mean value of K_{eff}.

Internal time scale t_r. In the ESC-model, the time scale is defined by the only combination with the time dimension, which is the retardation time $t_r = \eta / E_l$ of the Kelvin-Voight element. Both the viscosity η and rigidity E_l of this element are perhaps the most uncertain for rock. Meanwhile, the internal time is no more than a parameter ordering events in a sequence. Note also that according to (3.10), the mean time of aseismic events is characterized by $t_r / |\alpha|$ rather than t_r. Still, as in many cases the mean value of $|\alpha|$ is of order of unity, the retardation time is typical for the majority of aseismic events.

The contact viscosity η being uncertain, the time scale is conditional. Clearly, it should be less than a typical time step of the external time. It may be roughly estimated if a dependence of Omori type is available from observations.

Suppose we have dependence of the number of seismic events, occurred in equal time intervals after a strong excitation of rock (Figure 16*a*). The dependence is approximated by decaying exponent (Figure 16*b*) as

$$N_S = N_0 \exp(-t / t_O). \qquad (4.5)$$

Then we may associate the retardation time with the characteristic time t_O of the Omori dependence (4.5).

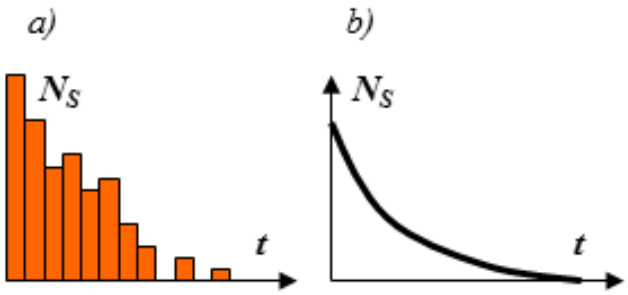

Figure 16. Dependence of Omori type for the number of seismic events after excitation of rock

Rigidity of Kelvin-Voight element E_l. It can be shown (Linkov[2006]) that for the distribution (3.12), the mean portion of accelerating events in the total number of all aseismic events is $1/2(M_c/E_l)/b_M$ if either (i) $1-a_M \le b_M$ and $a_M + M_c/E_l < 1$, or (ii) $a_M > 1$ and $1-a_M + M_c/E_l < b_M$. In these cases we may prescribe the rigidity E_l by choosing its value, which provides a needed portion of accelerating events.

Mean length of flaws l. The mean length l of seeded flaws may be defined via the expected level of energy W_l of events. Then, by using $a = l$ in (2.21), we obtain:

$$l = \frac{1.21\sqrt[3]{W_l}}{\sqrt[3]{K_{eff}(c_{0\tau} - c_{*\tau})^2/E}}. \qquad (4.6)$$

Note that the expression under the cubic root in (4.6) has the order of elastic energy released from a unit volume of rock under the stress drop $c_{0\tau} - c_{*\tau}$.

Flaw density ξ *and the number* N *of seeded flaws*. We have mentioned that the dominant factor causing chains of events is flaw interaction. The interaction is significant at distances less or comparable with the flaw minimal size *a*. Therefore, in problems concerning with modeling seismicity it is reasonable to introduce the flaw density as the ratio of the mean length l of flaws to the mean distance L between them:

$$\xi = \frac{l}{L}. \qquad (4.7)$$

In a 3D volume V with uniform distribution of N flaws, the mean distance between their centers is:

$$L = \sqrt[3]{\frac{V}{N}}. \qquad (4.8)$$

From (4.7) and (4.8) we obtain the total number of flaws to be seeded in a volume V to have the density ξ:

$$L = \sqrt[3]{\frac{V}{N}}. \qquad (4.9)$$

When using (4.9) we need to specify the range of the density, in which interaction of flaws is strong enough to produce chains of events while it is not too strong to lead to a chain reaction. For 3D problems, the range was established by numerical experiments (Linkov[2006]). It is:

$$0.14 < \xi < 0.75. \qquad (4.10)$$

When the density is below the lower threshold, there is actually no flaw interaction. Consequently, there are no chains of events. When the density is above the upper threshold, the interaction becomes so strong that there arise chain reaction involving almost all the seeded flaws into deformation.

A particular value of the density in the range (4.10) may be chosen from additional considerations. Consider rare strong events with the energy W_{str} notably, say 200-fold, exceeding the mean energy W_l. The number N_{str} of such strong events is first units, say $N_{str} = 1$. Then assuming the number of seismic events proportional to the number of flaws capable to produce events of prescribed energy, we have from (2.21) and (4.1) the expected number N_S of all seismic events:

$$N_S = N_{str} \exp\left(\sqrt[3]{\frac{W_{str}}{W_l}}\right). \qquad (4.11)$$

Naturally, the total number of seeded flaws should be at least an order greater than the expected number of seismic events. Denote k_N the fraction of flaws, which produce seismic events, so that $N = \frac{1}{k_N} N_S$. When using (4.11), we obtain the estimation:

$$N = \frac{1}{k_N} N_{str} \exp\left(\sqrt[3]{\frac{W_{str}}{W_l}}\right). \qquad (4.12)$$

When having N, Equation (3.19) defines $\xi = l\sqrt[3]{N/V}$. The found ξ should be within the range (4.10).

For a particular problem, the number k_N is not known in advance. Consequently, there might be need to perform a series of calibrating runs with a computer code. They start from a guess regarding k_N. Then for a prescribed ratio W_{str}/W_l, the value of N becomes available from (4.12) and (4.9) serves to find the density ξ. (The latter should be within the range (4.10)). The first run provides the portion k_N of flaws, which produce seismic events. The found k_N serves for the next run and so on. If at some step the density is outside the range (4.10), we need to repeat calibration by taking another value of N_{str}, say 0.1, or 2, or 5. Another, although limited option, consists in changing the volume V of seeded flaws. Finally we obtain the needed values of N and ξ.

Comment. Calibration is notably simplified when having the dependence frequency-magnitude of Gutenberg-Righter type obtained from field observations. We shall discuss this dependence below in Section "Output Data".

INITIALIZATION AND TIME STEPS

Initialization

The generated input data on flaws are firstly analysed on the initialisation step of calculations. As mentioned, it consists in considering in situ state of rock and exclusion those of seeded flaws, for which in situ tractions exceed the tensile or shear strength of a flaw. It is done by a subroutine, which we have called "ExclusInSitu". It presents a cycle over N seeded flaws with checking for each of them if its strength is exceeded. These flaws are excluded from further calculation and the number N is respectively diminished. The remaining flaws are assumed *active* in the sense that they are closed and able to experience seismic or aseismic DD under induced tractions.

Steps in External Time

After the initialisation, the code starts calculations in a cycle of external time steps. At the beginning of a step, a conventional (basic) code calculates tractions at the location of each active flaw. For brevity, we call them '*conventional tractions*'. Besides those, there arise additional tractions caused by the DD on flaws, which have been activated on previous steps. We call their sum at each of the current active flaws '*flaw-tractions*'. At the beginning of the first step, the flaw tractions are zero.

We neglect the back influence of the flaw-stresses on the conventional stresses. This serves us to use the basic code unchanged. Normally, it does not lead to notable loss of accuracy. Still, if there is need, the back influence may be accounted for by an iteration included into the basis code.

At each of the time steps, we perform calculations in a similar way. It is done by a subroutine, which we call "SeismTimeStep".

Consider a typical time step. For it, we have conventional and flaw-tractions at flaws, which are active to the beginning of the step. Calculations always start from the *zero-stage* and may include a number of *stages* depending if there arise *aseismic* events. Specifically, if there appear *aseismic* events on the zero stage, it is followed with the fist stage. If on the first stage there appear new *aseismic* events, it is followed with the second stage, and so on until aseismic events cease to appear. The calculations are performed as follows.

Zero-stage. At each active flaw, we add the flaw-tractions to the conventional tractions and check if the summary tractions exceed the tensile or shear strength. If the strength is exceeded, we calculate the DD arising at the flaw by using Equation (2.15) for the tensile mode, and (2.17) for the shear mode. Besides we check if the corresponding event is seismic or aseismic.

Then common quadratures of the H-BEM provide stresses caused by these DD at any point of a medium (see, e.g., Linkov *et al*.[1997]). The calculation is performed by a subroutine, which we call "TracFlaw3D". As a result, we obtain *additional* tractions caused by the DD arisen at an activated flaw at locations of other active flaws. The additional tractions are summed and stored *separately* for seismic and aseismic events, which have appeared on the zero-stage.

After checking all the active flaws, those of them, which have produced *seismic* events, are excluded from active and declared *passive* flaws. The sum of their additional tractions is immediately added to flaw-tractions. Then we start the next *cycle*, repeating the same calculations for the new set of active flaws and with updated flaw-tractions.

The cycles are repeated until new *seismic* events cease to appear. Then we turn to the flaws, which produced *aseismic* events. Now we exclude them from active flaws, declare them passive and add the sum of tractions induced by them to flaw-tractions. The stage is over.

First and following stages. The new sets of active flaws and flaw-tractions are used in the same way as that described for the zero-stage. If there arise new seismic events, we consider them appeared after those, which have been simulated on the previous stage. The time lag is assumed to be equal to the characteristic time of aseismic events. In this case, the Omori-type dependence may be modelled.

The stages are repeated until new *aseismic* events cease to appear. Then the current time step is over, and we may start the next step of external time.

Saved Information

In time steps, a computer code saves data on each event, seismic or aseismic, simulated. The information on an event includes:

1) Its number in the numeration of events in the sequence of their arising; the number of the flaw (in initial numeration of the flaws), on which it appeared; the input data for the flaw gives location of the event, orientation of its plane and prescribed mechanical properties.

2) The time step, at which the event is simulated.

3) The type of the event, seismic or aseismic. For a seismic event, its mode, tensile or shear. For an aseismic event, its character, accelerating or damping.

4) The stage within the time step, on which the event occurred.

5) The cycle (for a seismic event) within the stage, on which the event occurred.

6) Characteristics of a seismic or aseismic event, described in previous sections.

These data are sorted and analysed by output subroutines.

OUTPUT DATA

General Considerations

Simulation of events notably extends data on a rock mass state. In addition to common mechanical data on stresses, strains and displacements, provided by a conventional code, we obtain data on seismic and aseismic events caused by changes of stresses. These data are similar to those observed in mines or around a hydraulic fracture, or oil (gas, heat) production well. Specifically, we obtain data on temporal and spatial distributions of events. For each simulated seismic event, we have its mode (tensile or shear), coordinates of its source, orientation of the plane, nodal planes, DD, energy, seismic moment, seismic efficiency, stress drop and seismic shear. For each aseismic event, we have its type (accelerating or damping), time and stage of its occurrence, characteristic duration, stress drop and final shear DD. What is of special significance, in contrast with observed seismicity, for any event, we exactly know the mechanical state, at which the event occurred.

These data on events, placed in output files, undergo statistical processing. The latter may include building the tallies of the listed output characteristics; graphical plotting of Gutenberg-Righter and Omori dependences; delineation of regions of seismicity concentration such as pillars, edges of seams, moving front of a propagating hydraulic fracture, etc. This is done by postprocessor subroutines, which we assume joined in a single subroutine, called "FlawOutput". Consider some of post processing actions applied to mining and hydraulic fracturing.

Frequency-Magnitude Dependence

The frequency-magnitude dependence presents logarithm of the number N_W of seismic events with the magnitude exceeding m_W. According to Salamon[1993], the magnitude of a seismic event in Gutenberg-Righter scale is connected with the energy W measured in MJ, as:

$$m_W = 2/3(\log W + 1.2). \qquad (6.1)$$

A typical graph of the frequency-magnitude dependence is shown in Figure 17 by the solid line. It is obtained when simulating seismicity in a deep gold mine of South Africa (Linkov[2006]). The simulation is performed for mining conditions similar to those, for which summarised data of seismic observations are available (data by Anderson reproduces by Napier[2001]). The dashed line in Figure 17 shows the curve for observed events. The agreement looks impressive.

Note that in mining practice there are actually no events with the magnitude exceeding 2. This explains the drop of the curve near m_W = 1.5. On the other hand, there are very many events with small magnitude (m_W < 0), which are not accounted for in earth seismology. This explains close to horizontal part of the curves at small magnitudes. The average slope of the curve is close to -0.5. It is in contrast with the earthquake observations, for which the Gutenberg-Righter dependence is close to a straight line with the slope -1.

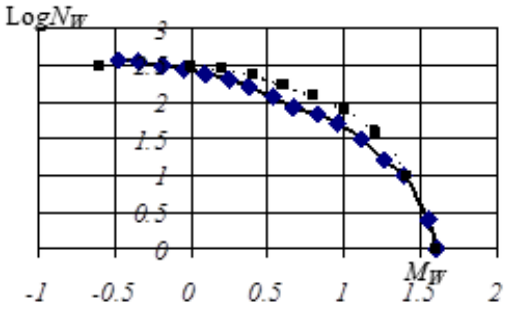

Figure 17. Dependences of Gutenberg-Righter type

For simulated seismicity, accompanying hydraulic fractures, the frequency-magnitude dependence is similar to that shown in Figure 17, but the magnitude of the strongest events is four orders less (Dobroskok and Linkov[2008]). It is because the net-pressure, which causes the fracture propagation and defines the change of stresses, is two-three orders less than the stress change induced by mining in deep gold mines.

Omori Dependence

Numerical simulation of exponentially decreasing number of seismic events after a strong excitation, corresponding to the stope advance in time, has led to an unexpected result (Linkov[2005, 2006]). It appeared that to simulate the Omori dependence (Figure 16), it is necessary to seed at least two sets of flaws with different linear scales.

One of them contains flaws having mean length of order of ten meters; the other is of the mining step (first meters). The Omori dependence arises as the influence of rare aseismic events, generated by large flaws of the first group, on small flaws of the second group, which generate the majority of seismic events. Figure 18 presents typical results obtained in this way for long-wall advance in three time steps. It shows the numbers of events at stages within each of the time steps.

Joined Geomechanical and Seismic Modeling and Monitoring

In the Introduction we have mentioned about the need and easy implementation of joined geomechanical and seismic modeling and monitoring. Figure 19 shows the distribution of projections of simulated seismic events to the horizontal mining plane when the long-wall mining advances 10 meters downward (along the x_3-direction). The solid line shows the contour of the mined area at the end of a mining step. Evidently, the events follow the change of the geometry.

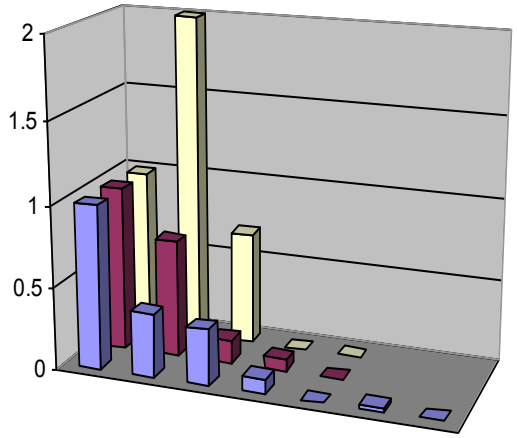

Figure 18. Numbers of seismic events on stages within three time steps

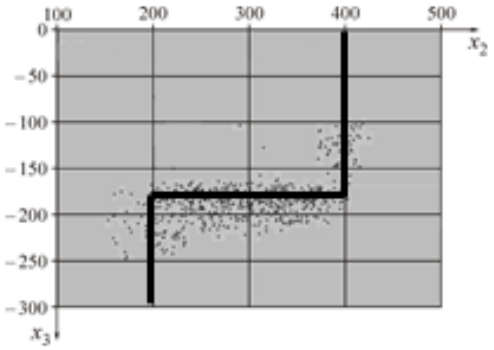

Figure 19. Projections of simulated seismic events to the mining plane

The distribution of the events in the vertical cross-section orthogonal to the mining line is shown in Figure 20. We may see that the simulated events group near the mining front. They are distributed in the roof and floor mostly beyond the wedge-like zone.

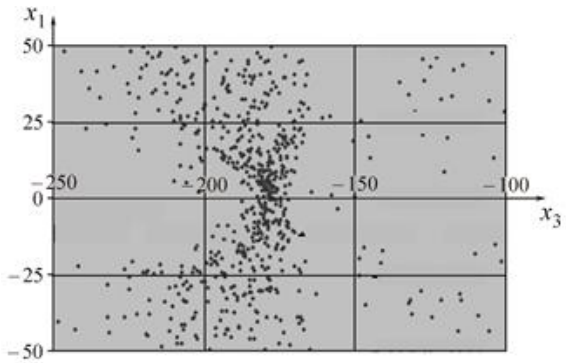

Figure 20. Projections of simulated seismic events to the vertical plane orthogonal to the mining line

Remarkably, almost no events occur in the seam just ahead of the mining front. The reason is that the shear stresses are small along the middle plane of the seam what prevents shear events. Meantime, calculation of mechanical quantities shows that the concentration of compressive normal stresses in this zone is very high. It implies that this zone is extremely dangerous as concerns with unfavorable manifestations of rock pressure.

The example clearly demonstrates that there are cases when seismic monitoring alone is not sufficient for obtaining reliable practical conclusions. The need to compare the observed seismicity with simulated events and to compliment it with geomechanical modeling is obvious.

Validation and Calibration of Input Data

We have already mentioned about extreme value of direct observations of seismicity for proper prescribing the input parameters on the seeded flaws. They are also important for improving a geomechanical model. For instance, the observed seismicity may serve to disclose important geological features like faults, dykes, zones of significant changes of mechanical properties and input data on in-situ cracks.

An impressive example of the kind is application of the unconventional fracture model (UFM) to numerical modeling of hydraulic fractures in low-permeable shales (Cipolla *et al*.[2007]). The input data of the numerical method, based on the UFM, include parameters on the supposed in-situ crack net in the area of simulation. These parameters are calibrated after obtaining data on spatial distribution of seismicity observed during hydraulic fracturing. Presently the method does not employ synthetic seismicity. Surely its reliability will increase when complimenting calculations of conventional mechanical quantities with numerical modeling of seismicity.

Inversion of Simulated Data. PCA and SRS Methods to Delineate Geometrical Features

For events simulated as described in the previous section, we know exact geometry, calculated stresses, strains, DD and displacements on time steps. Thus there is explicit correspondence between seismicity and mechanical quantities.

Forget, for a while, the knowledge on the geometry and mechanical quantities. Now we have only seismic data similar to that observed in rock. Consequently we may apply methods, used in mining practice for interpretation of observed seismicity, to the synthetic data. If the conclusions, obtained by a method of inversion, agree with the underlying mechanical state, the method is acceptable. Otherwise, it needs improvements.

Thus simulation of seismicity opens an opportunity for validation of existing methods of inversion. It may also serve for suggestion of new methods, adjusted to peculiarities of a particular problem (e.g. Dobroskok and Linkov[2008, 2009, 2011], Dobroskok *et al*.[2010]).

Consider, as an example, tracing of hydraulic fracture by employing seismic data on location and time of microseismic events.

Figure 21 presents projections of simulated events to the fracture plane. They were obtained in calculations for a fracture of the height 100 m propagating in 15 time steps, 10 m each. Thus the final fracture is a rectangle with the height 100 m and the length 150 m: $0 \le x_1 \le 150$, $-50 \le x_2 \le 50$. We may see that on whole the simulated events group within and near this rectangle.

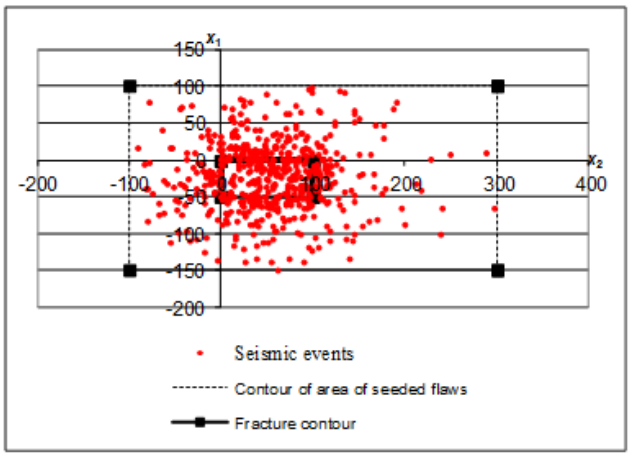

Figure 21. Projections of simulated seismic events to the plane of hydraulic fracture

Now we forget about the actual fracture plane and try to guess its position from the synthetic seismicity. To this end, we apply the method of strip ray scanning (SRS), specially suggested for tracing geometrical changes (Dobroskok and Linkov[2008]). The method employs counting simulated or observed events within a semi-infinite *strip* of a fixed width w_S and arbitrary orientation of the normal to the strip plane. The normal *scans* the hemisphere, and the orientation, corresponding to the maximal number of events within the strip, is associated with the normal to the plane containing the source, which induces the events (in the considered case, the fracture plane). Projections of the events to this plane are used for further analysis. We find tallies of events along various azimuths (*rays*) in the plane. The tallies contain information on geomechanical features within the plane. For instance, tallies obtained for a time step may serve to conclude on the position of the fracture front at this moment. Specifically, we may associate the tally having the most distinct peak with the direction of the front propagation. The most smeared tally, which normally corresponds to the orthogonal direction, is associated with the front line.

As an example, Figure 22 shows the tally of the events occurred at the sixth time step of simulated hydraulic fracture propagation. The actual position of the front is at the distance 60 m from the origin.

We may see that the maximal number of events remarkably agrees with the front location. The number of events ahead of the front does not differ significantly from their number behind the front. This means that in practice, the front line may be associated with the middle of events occurring per time needed for fracture propagation of about 10 meters. At least half of events are concentrated near the front line.

The conventional method of analyzing geometrical features is the principle component analysis, PCA (see, e.g. Jolliffe[1986]), currently employed in the oil (gas) production industry. It gives the orientation and three principal axes of an ellipsoid containing the majority of events. It does not provide tallies. The comparison of the PSA and SRS shows that when applied to the *totality* of the events, the both methods are capable to catch the mining or fracture plane with reasonable accuracy. However, the totality of events does not provide unambiguously estimation of the sizes of active zone (see, for example, Figure 21, where scattering of the events is notably out of the hydraulic fracture occupying the area $0 \le x_1 \le 150$, $-50 \le x_2 \le 50$).

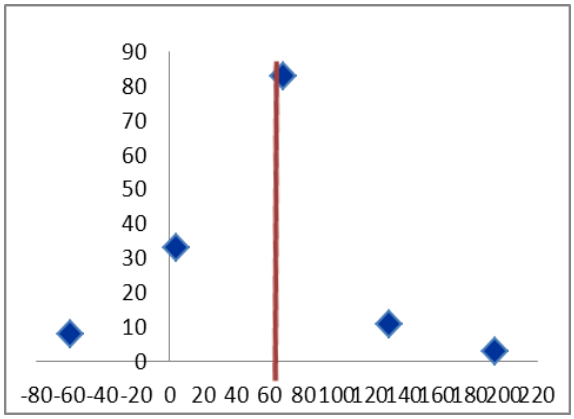

Figure 22. Tally of events simulated at the sixth time step of hydraulic fracture propagation

Further analysis shows that for tracing changes in geometry, it is much more informative to use statistically significant *groups* of events *on time steps*. Application of the PSA and SRS to these groups allows us to delineate the mining or fracture front and to find the direction of the propagation in time. The methods give close conclusions, when applied to the seismicity induced by long-wall mining. In contrast, the results for hydraulic fracturing indicate that the SRS is superior over the PCA. On the other hand, the PCA gives estimation of the strip width w_S, prescribed in the SRS. Thus taken together, the methods complement each other. Using the synthetic seismicity has allowed us to establish the accuracy, thresholds of applicability and relation between the methods.

Comment. Presently, in practice, only the totality of the observed microseismic events is used for making conclusions on a hydraulic fracture (e.g. Cipolla *et al.*[2011] and Wright[2007]). Meanwhile, the analysis based on numerical simulation of seismicity clearly shows the advantages of employing groups of events on time steps providing statistically significant number of events. It looks reasonable to use this conclusion in practice.

SUMMARY

We have presented an overview and new results on numerical modeling of seismic and aseismic events. The exposition explains how to adjust a conventional code of 3D BEM, FEM, DEM or other method to the modeling. It is sufficient to compliment a conventional code with a number of subroutines. They are conditionally named "FlawInput" for input data on seeded flaws; "ExclusInSitu", "SeismTimeStep" and "TracFlaw" for initialization and successive time steps; and "FlawOutput" for processing output data.

The results obtained to the date show the potential of the developed technique for better understanding processes in rock and for making practical decisions. The technique (with possible modifications) is applicable to various problems, in which events may occur at a wide range of scales: from microns in a brittle specimen to kilometres in the earth crust. Its implementation is quite simple and inexpensive. We suggest its employing to those who deal with brittle fracture accompanied with (micro)seismic events.

ACKNOWLEDGEMENT

The author appreciates the support of the European Research Agency (FP7-PEOPLE-2009-IAPP Marie Curie IAPP transfer of knowledge programme, Project Reference # 251475).

REFERENCES

AKI, K. and RICHARDS, P.G. *Quantitative seismology*, 2nd ed., University Science Books, Sausalito, CA, 2002. 700 p.

AL BUSADI, A., HAZARD, J.F. and YOUNG, R.P. Distinct element modelling of hydraulically fractured Lac du Bonnet granite, *J. Geophys. Res.*, vol. 110, 2005. p. B06302.

BELOV, E.B. and LINKOV, A.M. On instability conditions for softening on surfaces of a crack, *Researches on Building Mechanics and Constructions* (ed. Harlab, V.D.), St. Petersburg Institute for Architecture and Building, 1995. pp. 86–92 (in Russian).

CAI, M., KAISER, P.K., MORIOKA, H., MINAMI, M., MAEJIMA, T., TASAKA, Y. and KUROSE, H. FLAC/PFC coupled numerical simulation of AE in large-scale underground excavations, *Int. J. Rock Mech. Min. Sci. and Geomech. Abs.*, vol. 44, 2007. pp. 550–564.

CIPOLLA, C., WENG, X., MACK, M., GANGULY, U., GU, H., KRESSE, O. and COHEN, C. Integrating microseismic mapping and complex fracture modeling to characterize fracture complexity, in *Proc. SPE Hydraulic Fracturing Tech. Conf. and Exhib.*, The Woodlands, Texas, USA, 2011. 22 p.

COOK, N.G.W. The failure of rock, *Int. J. Rock Mech. Min. Sci. and Geomech. Abs.*, vol. 2, 1965a. pp. 389–403.

COOK, N.G.W. A note on rockbursts considered as a problem of stability, *J. S. Afr. Inst. Min. Metall.*, vol. 65, 1965b. pp. 437–446.

DETOURNAY, E., PEARSON, J.R.A. and THIERCELIN, M. Modelling rock mechanical processes in petroleum exploration and production, *ISRM News J.*, vol. 1, 1992. pp. 17–20.

DOBROSKOK, A.A. and LINKOV, A.M. Numerical simulation of seismicity accompanying hydraulic fracture propagation, in *Proc. 42nd US Rock Mech. Symp.*, San Francisco, CA, USA, 2008. CD ROM. 6 p.

DOBROSKOK, A.A. and LINKOV, A.M. Joint numerical simulation of stress changes, acoustic emission and/or microseismicity, in *Proc. of 23rd Int. Conf. Math. Modelling of Solids and Constructions. Methods of Boundary and Finite Elements*, St. Petersburg, Russia, 2009. pp. 72–74.

DOBROSKOK, A.A. and LINKOV, A.M. Numerical approach to interpretation of acoustic emission occurring at different scales, in *Proc. of 38th Summer School-Conf.: Advanced Problems in Mech.*, Repino, St. Petersburg, Russia, 2011. pp. 121–126.

DOBROSKOK, A.A., LINKOV, A.M. and ZOUBKOV, V.V. On joint geomechanical and geophysical monitoring in mines, *J. Min. Sci.*, vol. 46(1), 2010. pp. 13–20.

DRAGERT, H., WANG, K. and JAMES, T.S. A silent slip event on the deeper Cascadia subduction interface, *Science*, vol. 292, 2001. pp. 1525–1528.

DU, J., WARPINSKI, N.R., DAWIS, E.J., GRIFFIN, L.G. and MALONE, S. Joint inversion of downhole tiltmeter and microseismic data and its application to hydraulic fracture mapping in tight gas sand formation, in *Proc. 42nd US Rock Mech. Symp.*, San Francisco, CA, USA, 2008. CD-ROM. 11 p.

GIBOWICZ, S.L. and KIJKO, A. *An introduction to mining seismology*, Academic Press, San Diego, 1994. 399 p.

GREENGARD, L. and ROKHLIN, V. A fast algorithm for particle simulations, *J. Comp. Phys.*, vol. 73, 1987. pp. 325–348.

HUDSON, J.A., CROUCH, S.L. and FAIRHURST, C. Soft, stiff and servo-controlled testing machines: A review with reference to rock failure, *Eng. Geol.*, vol. 6(2), 1972. pp. 155–189.

FAIRHURST, C. Foreword to special issue: computers, rock mechanics and rock engineering, *Int. J. Rock Mech. Min. Sci. Geomech. Abs.*, vol. 25, 1988. pp. v–viii.

JOLLIFFE, I.T. *Principal component analysis*, Springer-Verlag, New York – Berlin – Heidelberg – Tokyo, 1986. 262 p.

KACHANOV, L.M. *Fundamentals of the theory of plasticity*, Dover Publications Inc., Mineola – New York, 2004. 478 p.

KAWASAKI, I. Silent earthquakes occurring in a stable-unstable transition zone and implications for earthquake prediction, *Earth Planet Space*, vol. 42(1), 2004. pp. 813–821.

KRESSE, O., COHEN, C. and WENG, X. Numerical modelling of hydraulic fracturing in naturally fractured formations, in *Proc. 45th US Rock Mech. Symp.*, San Francisco, CA, USA, 2011. p. 11.

LINDER, A.T., GLADWIN, M.T., JOHNSTON, M.J.S., GWYTHER, R.L. and BILHAM, A. Slow earthquake sequence on the San Andreas fault, *Nature*, vol. 383, 1996. pp. 65–68.

LINKOV, A.M. Stability of inelastic, geometrically nonlinear, discrete systems, *Soviet Physics Doklady*, vol. 32(5), 1987. pp. 376–378.

LINKOV, A.M. *Dynamic phenomena in mines and the problem of stability*, International Society for Rock Mechanics, Lisboa, Cedex, Portugal, 1994. 133 p.

LINKOV, A.M. Keynote address: New geomechanical approaches to develop quantitative seismicity, in *Proc. 4th Int. Symp. on Rockbursts and Seismicity in Mines* (eds. Gibowicz, S.J. and Lasocki, S.), Balkema, Rotterdam, 1997. pp. 151–166.

LINKOV, A.M. On modeling of slow and rapid processes in synthetic seismicity, in *Proc. 5th Int. Symp. on Rockbursts and Seismicity in Mines: Dynamic Rock Mass Response to Mining* (eds. van Aswegen, G., Durrheim, R.J. and Ortlepp, W.D.), Southern African Institute of Mining and Metallurgy, 2001. pp. 433–437.

LINKOV, A.M. Integration of numerical modeling and seismic monitoring: General theory and first steps, in *Proc. Int. Conf.: New Developments in Rock Mech.* (ed. Yunmei, L.), New York, 2002. pp. 259–264.

LINKOV, A.M. Numerical modelling of seismic and aseismic events in geomechanics, *J. Min. Sci*., vol. 41(1), 2005. pp. 14–26.

LINKOV, A.M. Numerical modelling of seismic and aseismic events in three-dimensional problems of rock mechanics, *J. Min. Sci*., vol. 42(1), 2006. pp. 1–14.

LINKOV, A.M., ZUBKOV, V.V. and KHEIB, M.A. A method of solving three-dimensional problems of seam working and geological faults, *J. Min. Sci.*, vol. 33(4), 1997. pp. 295–315.

LIU, Y.J. and NISHIMURA, N. The fast multipole boundary element method for potential problems: A tutorial, *Eng. Anal. Bound. Elem.*, vol. 30, 2006. pp. 371–381.

MALAN, D.F. and SPOTTISWOODE, S.M. Time-dependent fracture zone behavior and seismicity surrounding deep level stoping operations, in *Proc. 4th Int. Symp. on Rockbursts and Seismicity in Mines* (eds. Gibowicz, S.J. and Lasocki, S.), Balkema, Rotterdam, 1997. pp. 173–177.

MAXELL, S.C. and URBANCIC, T.I. The potential role of passive seismic monitoring for real-time 4D reservoir characterization, in *Proc. SPE Reservoir Evaluation and Eng.*, 2005. pp. 70–76.

MENDECKI, A.J. *Seismic monitoring in mines*, Chapman and Hall, London, 1997. 261 p.

NAPIER, J.A.L. Scale effects in the numerical simulation of time-dependent mine seismic activity, in *Proc. Int. Conf.: Rock Mech. in National Interest* (eds. Tinucci, J. and Heasley, J.), Swets and Zeilinger Lisse, 2001. pp. 1297–1304.

NAPIER, J.A.L. and MALAN, D.F. A viscoplastic discontinuum model and time-dependent fracture and seismicity effects in brittle rock, *Int. J. Rock Mech. Min. Sci. and Geomech. Abs.*, vol. 34(7), 1997. pp. 1075–1089.

RICE, J. The mechanics of earthquake rupture, *Phys. Earth's Interior* (eds. Dziewonski, A.M. and Boschi, E.), Elsevier, New York, 1980. pp. 555–649.

ROKHLIN, V. Rapid solution of integral equations of classical potential theory, *J. Comp. Phys.*, vol. 60, 1983. pp. 187–207.

SALAMON, M.D.G. Keynote address: Some applications of geomechanical modelling in rockburst and related research, in *Proc. 3rd Int. Symp. on Rockbursts and Seismicity in Mines* (ed. Young, P.), Balkema, Rotterdam, 1993. pp. 297–309.

SELLERS, E.J. and NAPIER, J.A.L. A point kernel representation of large-scale seismic activity in mining, in *Proc. 5th Int. Symp. on Rockbursts and Seismicity in Mines: Dynamic Rock Mass Response to Mining* (eds. van Aswegen, G., Durrheim, R.J. and Ortlepp, W.D.), Southern African Institute of Mining Metallurgy, 2001. pp. 405–411.

SPOTTISWOODE, S. Keynote address: Synthetic seismicity mimics observed seismicity in deep tabular mines, in *Proc. 5th Int. Symp. on Rockbursts and Seismicity in Mines: Dynamic Rock Mass Response to Mining* (eds. van Aswegen, G., Durrheim, R.J. and Ortlepp, W.D.), South African Institute of Mining and Metallurgy, 2001. pp. 371–377.

STARFIELD, A. and CUNDALL, P.A. Toward a methodology for rock mechanics modelling, *Int. J. Rock Mech. Min. Sci. and Geomech. Abs.*, vol. 25, 1988. pp. 99–106.

VAN DER MERWE, N. Time – the conventionally ignored dimension, *ISRM News J.*, vol. 2(3, 4), 1995. p. 57.

WILES, T., LACHENICHT, R. and VAN ASWEGEN, G. Integration of deterministic modeling with seismic monitoring for assessment of rockmass response to mining, in *Proc. 5th Int. Symp. on Rockbursts and Seismicity in Mines: Dynamic Rock Mass Response to Mining* (eds. van Aswegen, G., Durrheim, R.J. and Ortlepp, W.D.), Southern African Institute of Mining and Metallurgy, 2001. pp. 379–387.

WRIGHT, C. Case study: HDTV versus early television– you get to choose, *Pinnacle Newsletters*, 2007(spring). p. 4.

YING, L., BIROS, J. and ZORIN, D. A kernel independent fast multipole algorithm, *Technical Report TR2003-839*, Courant Institute, New York University, 2003. 31 p.